Fuel 220 (2018) 692–705

Contents lists available at ScienceDirect

Fuel

journal homepage: www.elsevier.com/locate/fuel

Full Length Article

Relaxation and relaxation exchange NMR to characterise asphaltene adsorption and wettability dynamics in siliceous systems

Igor Shikhov, Rupeng Li, Christoph H. Arns*

School of Petroleum Engineering, The University of New South Wales, Sydney 2052, NSW, Australia

ARTICLE INFO

Keywords:
Asphaltene adsorption
Clogging
Rock ageing
Wettability alteration rate
T2 relaxation
REXSY
v1

ABSTRACT

The fraction of asphaltenes in crude oils is among the major concerns in upstream and downstream petroleum engineering. At reservoir scale asphaltenes may cause compartmentalisation and at pore scale they may create barriers to flow, change wettability conditions and relative permeability; and as a result affect ultimate oil recovery. Rock core ageing in oil is a common step in laboratory core analysis. Where possible, crude oils relevant to the origin of cores are used, while the use of arbitrary oils, various hydrophobic chemicals and anti-wetting agents is not uncommon. Published ageing time and temperature vary broadly. This fact motivates us to evaluate the applicability of synthetic oils for studies requiring wettability alteration. We systematically study the precipitation kinetics of the heavy-end oil fraction and wettability alteration properties of mixtures comprised by various proportions of commercially available bitumen, aromatics and alkane components.

Low-field NMR relaxation measurements have been applied to characterise wettability of rocks by introducing an NMR wettability index. The latter requires multiple reference measurements at end-point saturation states similar to a standard Amott-Harvey workflow. Furthermore, petrophysical interpretation of T_2 relaxation data is prone to be affected by diffusional coupling effects. NMR correlation techniques have a higher prediction capacity, e.g. the T_2-store-T_2 (REXSY) experiment is naturally sensitive to the spatial variation of physical properties by detecting diffusion exchange between different relaxation environments. We applied a combination of relaxation and relaxation exchange techniques to study the effect of asphaltene deposition on pore-space morphology and wettability for two siliceous systems with different surface topology. The change of wettability over ageing time in different synthetic oils was tracked using T_2 relaxation measurements, providing estimates of ageing dynamics useful in designing wettability-related experiments.

Results show that the kinetics of asphaltene deposition and wettability alteration processes are strongly dependent on chemical composition of synthetic oils, asphaltene origin (light oil or bitumen) and solid phase morphology. Elements of the resulting deposition pattern and wetting state of the cores were inferred using the proposed approach, utilising low-field NMR T_2 relaxation and T_2-store-T_2 relaxation exchange experiments combined with numerical simulation of relaxation responses. The knowledge of deposition pattern and dynamics obtained mainly by the mean of combination of NMR relaxation techniques contributes to the improved design of core wettability alteration steps and potentially to enhanced petrophysical application of low-field NMR technology.

1. Introduction

1.1. Asphaltenes

Asphaltene dynamics in crude oils are among the major problems in petroleum engineering. The list of problems range from well completion using oil-based mud, pressure depletion and other situations leading to asphaltene precipitation onset conditions during production and transport in surface pipes. Wetting properties of natural rocks motivate studies of mechanisms governing wettability change and relationship to rock petrophysical properties; detection techniques and methods allowing to reproduce/control wettability change and associated chemical processes at reservoir conditions. Asphaltene is a heavy-end polar fraction of crude oils made of carbon, hydrogen, nitrogen, oxygen, sulfur and trace amounts of metals, operationally defined as the insoluble fraction of oil in light alkane and soluble in basic aromatic solvents [1]. Asphaltene dynamics represents complex processes considering their flocculation/aggregation behaviour,

* Corresponding author.
E-mail address: c.arns@unsw.edu.au (C.H. Arns).

https://doi.org/10.1016/j.fuel.2018.02.059
Received 28 September 2017; Received in revised form 16 December 2017; Accepted 8 February 2018
Available online 22 February 2018

interaction with other fluid components and various minerals. On the molecular level asphaltene dynamics can be described using the Yen-Mullins model [2], which assumes the basic structure of asphaltene molecule as a single moderately large polycyclic aromatic hydrocarbon with peripheral alkanes. The model postulates a two-step aggregation mechanism of basic asphaltene molecules: formation of small nano-aggregates and further clustering of these aggregates. In this work, however, we focus on scales far larger than molecular, i.e. on the effect of pore-scale asphaltene-to-solid interaction, and the deposit accumulation rate in rock void space depending on oil composition and the effect of deposits on wettability.

1.2. Wettability reversal/alteration in SCAL (ageing)

Wettability is a mutual solid-fluid property defined as the tendency of a fluid to spread over or adhere to a solid surface in the presence of other immiscible fluid(s). Wettability is one of the factors governing oil recovery since it controls initial fluid distribution, capillary pressure and relative permeability. It is a multi-scale phenomenon depending on mutual intermolecular interactions between the fluids and the solid, chemical potential of components, excess of free energy in solid (surface energy) and surface roughness (topology). The wetting properties of rocks in the context of petroleum engineering are considered qualitatively to be between strongly water-wet and strongly oil-wet states or a combination (mixed-wet). These states are quantified either through contact angle (which is a microscopic property) or through one of wettability indices, which relate observable change of saturation and saturation history to rock wetting capacity (macroscopic average property), such as the Amott method [3], the US Bereau of Mines (USBM) method and wettability index from pseudo work of imbibition w_R [4]. Among the alternative approaches is the direct measurement of zeta potential [5]. In this work we use a simplified approach to observe a wettability state of aged cores by measuring volume of self-imbibed heavy water into decane-saturated cores.

Core analysis in the context of evaluation of reservoir quality requires the restoration of a core's wettability state. This is typically performed by setting a core to strongly water-wet state using a variety of cleaning procedures and subsequent alteration of the core wettability to some degree of oil wetness. The latter can be achieved using special hydrophobic chemicals and anti-wetting agents (such as dimethyldichlorosilane) [6]. Alternatively, a so-called ageing process is used – exposure of the rock to crude oil at elevated temperature. Where possible, crude oils native to core samples are used. However, in many cases, the selection of oil is arbitrary, which complicates comparison of results. Furthermore, while the role of asphaltenes in wettability reversal is long known [7], the possible heterogeneous wettability as an outcome of ageing in crude oil has been previously reported by Graue et al. [8]. We study the effect of oil composition on precipitation kinetics of asphaltenes and relationship between NMR surface relaxivity and wettability alteration.

1.3. NMR applications to wettability

Low-field NMR relaxometry is a powerful tool for non-invasive studies of molecular dynamics in porous systems suitable to deal with paramagnetic environments such as natural rocks. Accordingly, it is commonly applied for the petrophysical characterisation of rocks. It has sensitivity to the wetting state of rock through the effect of surface relaxivity, which lead to the proposal of NMR indices correlating very well to standard USBM index [9,10] and to Amott index [11,12]. Further improvements were achieved with the aid of numerically modelled NMR response using simplified pores geometries [13]. These models assume homogeneity of surface relaxivity and wettability. However, the impact of wettability heterogeneity on relative permeability is long known, [14]. The effect of surface relaxivity heterogeneity was investigated numerically using simulated NMR relaxation experiments and 3D micro-CT representations of rock and various patterns of relaxivity distribution by Arns et al. [15], who demonstrated that heterogeneity of surface relaxivity affects NMR permeability cross-correlations by weakening correlation between porosity and log-mean relaxation time. Using an analytically derived model for rectangular pores, a framework to estimate the influence of spatially variable relaxivity on observed NMR responses in rocks has been proposed [16]. Systematic experimental studies of surface relaxivity heterogeneity on relaxation rates using sandpacks altered with ferrihydrite were conducted by Keating and Knight [17]. Clearly, the variations of wettability of a given mineral constituent of the rock correspond to variations of surface relaxivity. It is less obvious how the precipitation of asphaltenes following various scenarios (favouring pore topology or mineralogy or combination of both) would affect such interpretation. Low-field NMR relaxometry as employed in this study is not sensitive enough to provide direct insight into the molecular structure of asphaltenes nor reliably measure their quantity even at short echo-spacings of 80 μs. Nevertheless, it can be used to indirectly detect the presence and distribution of asphaltene floccules through the effect of their interaction with saturating fluid.

1.4. Distribution and rate of asphaltenes deposition

Asphaltene adsorption on solid surfaces in rocks is considered to be a major cause of wettability reversal inside oil reservoirs [18]. Another effect of asphaltene deposition is porosity and permeability reduction [19]. Asphaltenes are likely to precipitate on rock surfaces non-uniformly, depending on mineralogy, pore shape and surface roughness. Understanding of the influence of these factors would assist in improving multiphase flow models. In favourable conditions (low asphaltene concentration, strong aromatic solvent, surface with uniform and strong affinity) the sorption process follows a simple adsorption isotherm (Langmuir or type I according to IUPAC [20]), which corresponds to homogeneous monolayer formation. In less favourable conditions (high asphaltene concentration, poor solvent) multilayer formation is observed and various adsorption regimes may co-exist correlating to the degree of asphaltene aggregation, which can result in very high specific adsorption values q_a reported in units of $[mg/m^2]$. A variety of scenarios are covered by IUPAC type II to type V adsorption isotherms. No single analytical expression so far have been offered to cover all variants of sorption processes. The Fowler and Gugge140 nheim [21] model covers three types of isotherms: the mentioned type I, type III - pure multilayer formation without saturation limit and type V, which allows lateral interaction and includes capillary condensation effects. Characteristic qualitative difference of these scenarios result in either Γ-, *J*- or *S*-shape of an adsorption-equilibrium concentration trend (q_a vs C_{eq}) and also are expected to appear in deposition kinetics, whichever form is used: specific deposit mass per unit surface area $q_a(t)$, coverage $\theta_a(t)$ or occupied pore-space fraction, $d\phi_\delta(t)$.

Many techniques and their combinations have been applied to characterise asphaltene deposition. A study based on SEM and pressure drop in capillary allowed to conclude that submicron asphaltene aggregates are likely responsible for fouling [22]. A work based on optical microscopy/photomicrography techniques concluded that the deposition rate depends mainly on oil/n-alkane ratio and alkane carbon number [23]. 3D optical microscopy was used to investigate effects of carbon dioxide on asphaltene deposition at various pressures by detecting size of asphaltene aggregates and glass surface area covered by deposit [24]. It also was applied to measure a deposition rate in a glass microchannel as a function of pumped volume at a constant and variable flow rates [25]. It was established that the type of n-alkane and oil in the mixture governs the resulting thickness of a deposit. However, since experiments were carried out over limited time intervals (several hours), even qualitative predictions about the long-time dynamics are not possible. This signifies the importance of long time adsorption behaviour in asphaltene-solid systems.

High resolution micro-CT tomography have been applied to directly detect and quantify deposits, dedicated to the impact of asphaltene precipitation in sandstone during CO_2 flooding [26] A combination of several techniques were applied by Kumar and Fogden [27]: micro-CT – to determine oil and water distribution within pore space, FESEM – to evaluate asphaltene deposition and optical profilometry – to obtain 3D surface maps. Wetting characteristics of 55 crude oils and pure samples by measuring advancing contact angle values as function of ageing time were examined in [28]. Results clearly demonstrated that deposition of surfactants and asphaltenes gradually rendered the surface progressively more oil-wet with respect to time as the system aged. The process of contact angle change reached saturation in sandstone after 20 days and in carbonate after 50 days. Different behaviour of asphaltenes originating from heavy and light oils was reported in [29]. This signifies the importance of molecular-level studies targeting the influence of asphaltenes structure. In this study we used natural and synthetic oils containing asphaltenes originating from light oil and bitumen in ratios: 1:0, 0.6:0.4, 0.3:0.7 and 0:1. Below we discuss our observations whether these ratios correlate to the ageing process.

1.5. Scope of this work & workflow

The present work concerns about the impact of asphaltenes on rock petrophysical properties in the following areas:

- the rate of asphaltene deposition in sandstone saturated with various synthetic oils after ageing and cleaning cycles; influence of oil composition on ageing efficiency;
- the rate of wettability change and potential correlation to deposition rate; the effect of surface-to-volume, S/V (surface topology) on deposition rate and wettability change;
- the detection of asphaltene deposition and wettability change by combination of NMR T_2 relaxation and T_2 relaxation exchange NMR experiments; and
- the characterisation of mixed-wet systems.

We aged beadpacks and outcrop sandstone plugs with a variety of crude and synthetic oils to investigate the relationship between asphaltene accumulation and wettability change over time depending on oil composition. Wettability change was tracked by measuring NMR T_2 relaxation responses. Relaxation responses were also modelled using random walk simulation on high-resolution micro-CT images utilised as morphological inputs. To interpret results we modelled asphaltene deposition over time following two scenarios: (1) uniform random precipitation and corresponding change of surface relaxivity; (2) non-uniform, enhanced with increase of local surface-to-volume by applying morphological transformations to threshold adjacent pore space. We hypothesise that during the ageing process asphaltenes readily deposit in the following two environments: (a) in the high S/V pore space surfaces, pore crevices and kaolinite patches; (b) onto low S/V grain surfaces, likely with much slower rate if any solvent involved. Alternatively, deposition and change of wetness may occur uniformly on all solid surfaces as a thin layer. These scenarios can be expressed through (volumetric) material balance for asphaltenes phase as following:

$$V_{a,total} = M_{dep}/\rho_{m,a} = V_{agg} + V_{layer} = \phi_{asph}\, V'_{agg} + \theta_a\, A_{grain}\, \delta_{a,layer}, \quad (1)$$

where $V_{a,total}$ is the total volume of precipitated asphaltene, V_{agg} and V'_{agg} the volume of asphaltene accumulations in crevices (solid and bulk), V_{layer} corresponds to the volume of asphaltenes attached on the surface, A_{grain} is the surface area of grains, θ_a the surface fraction covered by asphaltenes, $\delta_{a,layer}$ the average layer thickness, $\rho_{m,a}$ the asphaltene density and ϕ_{asph} the porosity of aggregates.

We propose a workflow to obtain unknown elements of this deposition model, Fig. 1. Firstly, the weight of deposition M_{dep} and surface area A_{grain} of a porous system are to be obtained. The latter may vary by

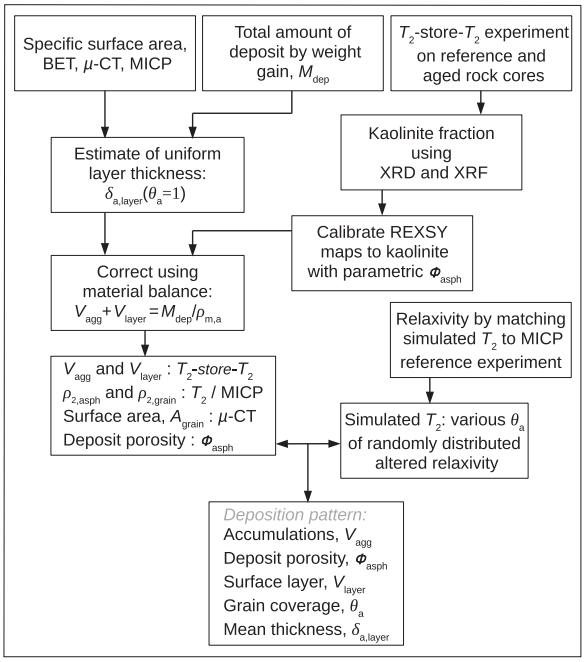

Fig. 1. Workflow diagram describing the proposed approach of evaluation of the asphaltene deposition pattern.

two orders of magnitude depending on the method: the specific surface area of Bentheimer sandstone using BET measurements (gas adsorption) was reported to be 1.3 m^2/g [30], while the value we derived from MICP measurements is just 0.5 m^2/g, close to 0.45 m^2/g reported in [31]. Another measure of surface area is micro-CT imaging, which is a strong function of resolution. It has been shown that the increase of resolution from 3.4 to 0.9 μm/voxel results in a 50-fold higher surface area for Bentheimer sandstone, [32]. However, the main contributors to additional surface area are clay and partially resolved grain contacts, which we intend to exclude. In the context of NMR relaxation it is worth noting that structural length scales smaller than 1 μm are diffusionally averaged out [33]. With the exception of clay bound water, the Bentheimer image at 3 μm/voxel adequately represents transport properties of a real rock [34]. Thus, while the specific surface area of the image is the lowest among other techniques (between 0.035 m^2/g [35] (assuming a bulk density 2.0 g/cc) and 0.015 m^2/g [36]), it is a suitable representation for deposition modelling. From Eq. (1) and surface relaxivity balance (the latter would ignore effects of clay and accumulations) the following estimate of coverage θ_a can be made: (Table 1)

$$\theta_a = \frac{V_{a,total} - V_{agg}}{\delta_{a,layer}\, A_{grain}} = \frac{\rho_2(t_a) - \rho_{2,grain}}{\rho_{2,asph} - \rho_{2,grain}}, \quad (2)$$

where $\rho_2(t_a)$ is the observed surface relaxivity at a given ageing state and $\rho_{2,grain}$ and $\rho_{2,asph}$ are the relaxivity of clean grain and of deposited asphaltenes respectively. The definition above has a lot in common with NMR wettability indices, e.g. [11], and can be treated as such. The fraction of asphaltenes deposited on the surface and accumulated as clusters can be determined from a T_2-store-T_2 experiment. Relaxivity is defined as a proportionality coefficient to (S/V) in the following equation describing relaxation as a linear sum of three independent processes (bulk, surface and diffusion) [37,38]:

$$\frac{1}{T_2} = \frac{1}{T_{2B}} + \frac{1}{T_{2S}} + \frac{1}{T_{2D}} = \frac{1}{T_{2B}} + \rho_2 \frac{S}{V} + \frac{D(\gamma G t_E)^2}{12}, \quad (3)$$

where γ is the poroton gyromagnetic ratio, D the diffusion coefficient, G the average magnetic field gradient and t_E the echo time. The surface relaxation in the equation is valid when fluid's spins are relaxing in the fast diffusion regime, for homogeneous surface relaxivity, negligible

Table 1
Table of symbols and abbreviations.

Symbol	Meaning
t_a	Ageing time
M_{dep}	Weight of deposited asphaltene
$\rho_{m,a}$	Solid asphalte density
$d\phi_\delta$	Percentage of porespace lost to deposition
ϕ_{asph}	Porosity of deposited asphaltene aggregates
$V_{a,total}$	Total volume of precipitated solid asphaltene
V_{agg}	Volume of solid asphaltene in aggregates
V'_{agg}	Bulk volume of aggregates, V_{agg}/ϕ_{asph}
V_{layer}	Volume of solid asphaltene in a layer
A_{grain}	Surface area of grains
q_a	Specific adsorption, mass per unit area
θ_a	Grain surface coverage by deposit
$\delta_{a,layer}$	Mean thickness of a deposit layer
ρ_2	Effective (observed) relaxivity
$\rho_{2,grain}$	Relaxivity of clean grain surface
$\rho_{2,asph}$	Relaxivity of deposited asphaltene
$d\rho_n$	Relative relaxivity change (aged/not-aged)

contribution of T_{2D} and the absence of diffusion coupling [39]. The surface relaxivity ρ_2 is an effective property of fluid-to-solid interactions attributed to the ability of a solid to enhance spin relaxation of a fluid. This property was introduced mainly for practical reasons to characterise saturated porous systems. Correspondingly, one of the possible definition reflects exactly this: The proportionality constant between T_2 decay time and pore size is called surface relaxivity [40].

We also use a relative relaxivity change $d\rho_n$ (a difference of relaxivity between the aged core and the reference non-aged, divided by the latter value, thus dimensionless) to correlate relaxivity evolution due to ageing with chemical composition of oils and rock porosity change.

2. Samples and preparation procedures

2.1. Fluids

In this study we used five oil mixtures composed by various proportions of bitumen of C170 grade, toluene, n-hexadecane and crude oil from one of the Asia-Pacific oil fields. The proportions of each component in oil mixtures are summarised in Table 2. Asphaltene fraction in these oils varies between 1.6 and 6.6 wt%, and fraction of resins varies from 3.4 to 17.4 wt%, Table 3. Oils OM.3 and OM.4 with the highest degree of resins and asphaltene content exhibit the highest viscosity and inversely, the lowest mean diffusion coefficient of 385 and 478 $\mu m^2/s$. The two oils, OM.0 and OM.1, with low resins and asphaltene content show the fastest mean diffusion coefficient of about 610 $\mu m^2/s$ (Table 4). All mixed oils are strongly diamagnetic exhibiting magnetic susceptibility values within a narrow range of -8.0 to -8.6 μSI. We expect very limited effects of internal gradients in diamagnetic rocks like clean sandstone saturated with pure hydrocarbon, crude or synthetic oil utilised in this study. Oils used for ageing, and n-decane used to saturate core plugs after ageing, were not de-oxygenated. The effect of oxygen on bulk relaxation time of fluids may be very substantial [41,42]. The relative contribution to total relaxation rate due to dissolved oxygen decreases in saturated porous systems with an increase of the surface relaxation component. However, it can be very different among rocks of different morphology and mineralogy. Since in this work a single rock is used, the effect of dissolved oxygen on results can be neglected.

Table 2
Components of five oil mixtures.

Synthetic oil	Bitumen wt%	Crude oil, wt%	$C_{16}H_{34}$ wt%	Toluene wt%
'OM.0'	5.0	30.0	30.0	35.0
'OM.1'	10.0	0.0	50.0	40.0
'OM.2'	15.0	30.0	15.0	40.0
'OM.3'	25.0	0.0	40.0	35.0
'OM.4'	41.7	0.0	0.0	58.3

2.2. Beadpacks and sandstone plugs

We prepared beadpacks made of borosilicate beads. The large diameter ($d = 1.532 \pm 0.110$ mm) was selected to reduce a possible capillary condensation effect on asphaltene precipitation. Six beadpacks underwent ageing in a crude and five different oil mixtures (crude oil, mixtures OM.0 to OM.4) at room temperature for 4 days, following 10 days of ageing at 60 °C. Then beads were cleaned in hexane, dried at 60°C for 24 h and packed in borosilicate bottles (Fig. 2[a–g]). Lastly, the beadpacks were saturated with n-decane.

We cored 38 Bentheimer plugs (32–34 mm long and 12.7 mm diameter): two reference cores, which were never exposed to oils and the other 36 were cleaned in methanol, dried and saturated with three types of synthetic oils (OM.1, OM.2. OM.3) using the desiccator/vacuum pump setup, 12 samples per each oil type. Aging has been performed over 12 time intervals following schedule shown in Table 5. The samples of resulting three sets were named as following: BH'*oil name* (*number*)'.'*time interval*', e.g. BH1.7, BH3.12, etc. The mean porosity of the 28 Bentheimer plugs is 23.88 ± 0.35%, permeability to brine measured on larger cores is 1.3 Darcy. Magnetic susceptibility of this rock is found to be weakly diamagnetic, about $-2\,\mu SI$.

2.3. Ageing/cleaning

Initially dry rock samples were fully saturated with a particular type of synthetic oil using a desiccator connected to a vacuum line. Samples were kept at room temperature for four days and in the end one sample was spared as underwent initial cold ageing step, though this time is counted in total time. Then we start ageing at elevated temperature of 60 °C following the schedule shown in Table 5. Accordingly, each sample was aged once for a scheduled ageing time interval. Lastly, the cores were cleaned by soaking in n–hexane at room temperature for six days, fluid was replaced every 12 h.

3. Experimental techniques

3.1. NMR relaxation and REXSY experiments

We use 2 MHz Magritek Rock Core Analizer to measure T_2 relaxation distributions of fluid-saturated cores with the standard Carr-Purcell-Meiboom-Gill (CPMG) technique [43,44]. The CPMG pulse sequence consists of a 90° pulse to place the magnetisation into the transverse plane following by a series (train) of 180° pulses to re-focus the signal. The time interval between adjacent 180° pulses is called echo time (t_E) and corresponds to the spacing between maxima of refocused signals. The timing between the initial 90° and 180° pulses is half the echo time. The top of each echo was acquired providing magnetisation decay (assumed to be multi-exponential). The inversion problem of obtaining regularised multi-exponential solution to a decay has been obtained with 1D inverse Laplace transform (ILT) with non-negativity constraint and L-curve smoothing criteria following [45,46]. Presented T_2 distributions were obtained with $t_E = 200\,\mu s$, Fig. 11[a–c]. The number of echos or echo-train length was selected to be long enough to resolve the longest relaxation component (bulk fluid). Experiments were repeated 16 times with a standard 4-step phase cycling sequence CYCLOPS (CYCLically Ordered Phase Sequence) [47] to suppress systematic noise due to imbalances in spectrometer hardware providing a SNR of about 110. The repetition time between scans was 60 s to maintain a constant temperature of the sample.

Table 3
SARA analysis of base hydrocarbons/mixtures and stability indicators.

Hydrocarbons	Saturates wt%	Aromatics wt%	Resins wt%	Asphaltenes wt%	Volatiles + LOC[a], wt%	Asphaltenes to Resins	CII index[b]
Crude oil	38.40	5.60	6.20	1.49	48.30	0.24	–
Bitumen	12.90	28.80	41.70	15.72	0.90	0.38	0.41
'OM.0'	42.17	38.12	3.95	1.23	14.54	0.31	1.03
'OM.1'	51.29	42.88	4.17	1.57	0.09	0.38	1.12
'OM.2'	28.46	46.00	8.12	2.81	14.63	0.35	0.58
'OM.3'	43.23	42.20	10.43	3.93	0.23	0.38	0.90
'OM.4'	5.38	70.31	17.39	6.56	0.38	0.38	0.14

[a] LOC – loss on column (mainly dissolved gas and light-end paraffins).
[b] CII (Colloidal Instability Index) = (Saturates + Asphaltenes) [wt%]/ (Resins + Aromatics) [wt%].

The T_2-store-T_2 experiment, Relaxation EXchange SpectroscopY (REXSY) was first introduced by Lee et al. [48] and later reintroduced [49,50] once fast 2D inverse Laplace transform algorithms became available [51]. It has been applied to the study hydration processes in cement pastes [52], bi-modal porosity synthetic systems (beadpacks) [53], biofouling in rocks [54] and sedimentary rocks [55]. Nevertheless, relative to other NMR relaxation and diffusion techniques REXSY saw rather a limited application being relatively time-consuming and demanding on high SNR since features of interest (cross-peaks) highly susceptible to artifacts and blurring caused by the ill-conditioned nature of the inversion (analysis of complexity and possible approach to treat the ambiguity was reported in [56]).

The REXSY experiment is designed to correlate bins of a $T_{2,a}$ spin relaxation distribution (i.e. i-th bin is $T_{2,a}(i)$) to the relaxation environments where spins will diffuse over a given time interval (another complete T_2 distribution, $T_{2,b}(i)$), which essentially creates a 2D correlation relaxation map. The T_2-store-T_2 pulse sequence is made of two CPMG pulse trains ($T_{2,a}$ encoding and $T_{2,b}$ recording relaxation domains) separated by a mixing time interval τ_m, Fig. 4. During the first encoding period spins situated in the initial relaxation environment will have its signal decay similar to an ordinary CPMG experiment. The length of this initial echo-train is selected to try every desired bin of a $T_{2,a}$ domain. Then, magnetisation is stored back along the longitudinal axis, experiencing reduced relaxation rate in most practical situations. During the following mixing time interval, the spin populations which have undergone relaxation in $T_{2,a}$, are allowed to diffuse, so that after time τ_m spins can be found in partially or completely different environments $T_{2,b}$. Finally, the diffused spin populations are measured with a full CPMG sequence and an amplitude at the top of each echo is acquired. A fast Laplace inversion numerical algorithm from Magritek was used to generate 2D relaxation distributions. One known issue with the technique is an uneven spatial base of $T_{2,a}$ and $T_{2,b}$ domains since spins experience diffusion over time of encoding and recording CPMG parts. This effect may lead to a lack of symmetry of acquired T_2-T_2 maps, which can be addressed with a sequence utilising an even spatial support base (at the expense of uneven echo-time in $T_{2,a}$ and $T_{2,b}$ parts) [50].

The nature of the REXSY experiment imposes a limitation on T_1/T_2 ratio, which should be $\gg 1$ for at least one of two environments [57]. In the limit of $T_1 = T_2$ there will be no exchange peak. Mixing time τ_m has to be selected to be reasonably long to enable diffusional exchange, but short enough relative to T_1 of the fast relaxation environment to allow the detection with the second echo-train. We performed REXSY with τ_m = 100 ms, 80 steps in $T_{2,b}$ domain, and t_E = 200 μs.

4. Modelling

4.1. Simulation NMR responses

The interpretation of NMR relaxometry in the context of rock morphology and asphaltene deposition/wettability relationship can be enhanced with the aid of simulated relaxation experiments, utilising a random walk technique on segmented tomographic images [58,59].

In the pore space, random walkers can progress towards any one of the six possible directions experiencing dephasing in internal gradients arising from different susceptibilities. The interaction between molecules and solid phases are simulated by assigning relaxivities to interfaces between different phases. Then we use a simulated CPMG technique to acquire the signals of an ensemble of spin-packets (isochromats) followed by inversion of the resultant magnetisation decay.

During the ageing process asphaltenes readily deposit in the following two environments: (a) in the high S/V pore space surfaces, pore crevices and kaolinite patches; (b) onto low S/V grain surfaces, however, with distinctively slower rate. Alternatively, deposition and change of wetness may occur uniformly on all solid surfaces as a thin layer (beyond typical micro-CT resolution of 3 μm/voxel). The degree of wetness change is controlled using a broad range of assigned surface relaxivity values. To test these two scenarios against observable NMR relaxation data, we mimic these by relabelling a segmented micro-CT image of Bentheimer sandstone accordingly. Initially we have three segmented phases: #1 void, bulk pore space; #2 clay patches assumed to have 50% unresolved porosity; #3 solids – quartz and feldspar

Table 4
Physical properties, Total Acid Number, Total Base Number and magnetic susceptibility.

Hydrocarbons	Density g/cc	Viscosity cP	Diffusion coef. D,μm²/s	TAN, mg KOH/g	TBN, mg KOH/g	Susceptibility χ_v,μSI
n–hexadecane	0.7713	3.25	402	–	–	−8.08
n-decane	0.7277	0.89	1328	–	–	−7.64
Toluene	0.8625	0.60	2163	–	–	−7.57
Crude oil	0.8134	16.41	198	1.19	0.66	−8.56
Bitumen	1.0304	–	–	1.90	3.80	−9.76
'OM.0'	0.8235	1.85	607	1.40	0.40	−8.22
'OM.1'	0.8240	1.78	610	1.63	0.32	−8.04
'OM.2'	0.8529	2.42	510	1.14	0.78	−8.27
'OM.3'	0.8792	3.61	385	2.37	1.00	−8.32
'OM.4'	0.9325	6.04	478	0.79	1.58	−8.48

Fig. 2. Reference 20 cc borosilicate beadpack [a] and beadpacks aged over 14 days in different natural and oil mixtures (dried): [b] OM.4; [c] OM.3; [d] OM.2; [e] OM.1; [f] OM.0; [g] crude oil.

Fig. 3. Images of Bentheimer cores aged in three synthetic oils (left to right: OM.1, OM.2, OM.3) over different time intervals: [a–c] 10 days; [d–f] 22 days, [g–i] 36 days and [j–l] 52 days.

Table 5
Ageing schedule of Bentheimer cores (at 60 °C).

Step/sample No	1	2	3	4	5	6	7	8	9	10	11	12
Time step, d*t* [hrs]	0	36	48	60	72	96	120	144	192	384	576	672
Time step, d*t* [days]	0	1.5	2	2.5	3	4	5	6	8	16	24	28
Hot ageing time, t_a [days]	0	1.5	3.5	6	9	13	18	24	32	48	68	96
Total ageing time, t_a [days]	4	5.5	7.5	10	13	17	22	28	36	52	72	100

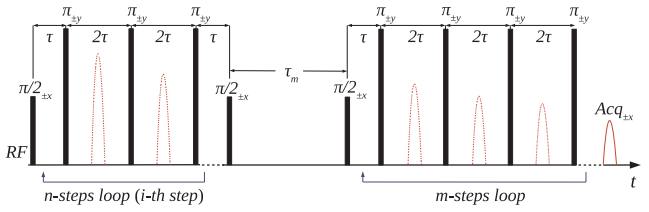

Fig. 4. Pulse sequence diagram of T_2-store-T_2 experiment correlating two relaxation dimensions $T_{2,a}$ and $T_{2,b}$ separated by a fixed exchange time τ_m.

grains. Two additional phases corresponding to asphaltene deposition during the ageing process are added as following: #4 – accumulations in high S/V regions of initially void space performed by relabelling part of phase #1 by thresholding a covering radius field (CRT, the maximum radius of the sphere, which can cover the voxel of a phase) [60].

The deposition process on low S/V surfaces is mimicked by creating an imaginary phase #5 at the expense of solid phase #3 (thresholded Euclidean Distance field, EDT – in our case a voxel layer normal to the solid phase surface). This new phase is combined with a uniform random voxelised field so that the total fraction of relabelled surface changes from 0% to 100% (Fig. 5[a–c]). These morphological operations enable us to reproduce a partial or complete (uniform) change of surface properties of a solid. The surface layer phase #5 receives no volumetric properties assignment, such as porosity, hydrogen index *HI* (#5) or own bulk relaxation response, $T_{2,B}$(#5). Selection of physical properties of various constituents of saturated rock for the purpose of NMR simulation is described in detail in the following section. Conceptual and actual spatial relaxivity assignments and corresponding simulated T_2 distributions for different relaxivity values different

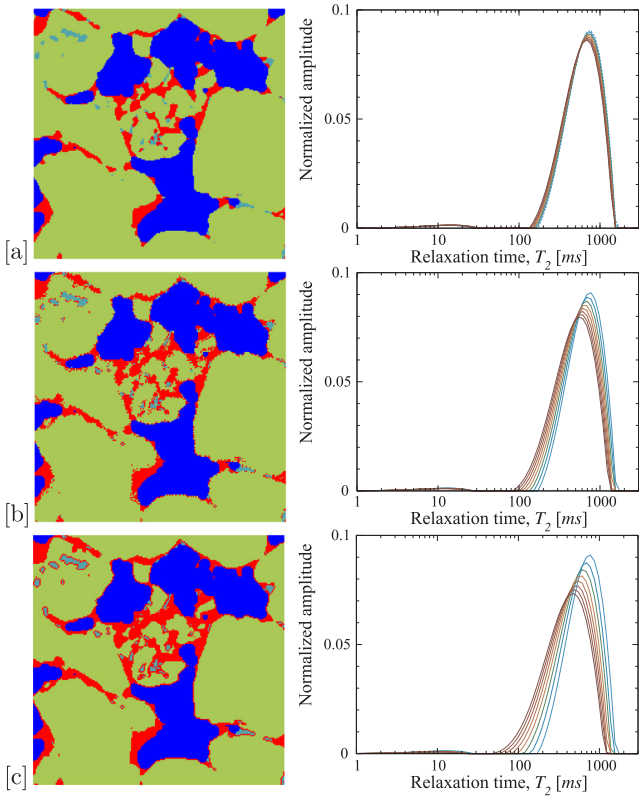

Fig. 5. *Left:* A slice of 1.2 mm × 1.2 mm field of view through the segmented Bentheimer micro-CT image altered using morphological transforms to mimic three asphaltene deposition scenarios: [a] deposition occurs in the pore crevices (high S/V) at the expense of pore space; [b] same as [a], in addition 50% of grain surface is randomly altered (accepts properties of asphaltenes, however, no volume assigned), labelled out from solid phase; [c] the grain surface is uniformly altered. *Colour legend*: blue – void/pore space #1; cyan - kaolinite #2; pale yellow - grains #3; red – deposition #4 and #5. *Right:* simulated T_2 distributions corresponding to scenarios [a–c]: each set of curves corresponds to grain surface relaxivity 4 μm/s and altered surface fraction of 10% [a], 50% [b], 100% [c] for which relaxivity vary between 4 and 18 μm/s with 2 μm/s increment.

wettability scenarios are shown in Fig. 5[a–c].

4.2. Input physical properties

Simulation of NMR relaxation requires a set of physical properties.

Table 6
Diffusion coefficient per phase, D_i [μm²/s].

Segmented phase	Void #1	Clay #2	Quartz #3	Deposit #4	Layer #5
Void #1 (macropore)	1250	575	0	575	0
Clay #2 (kaolinite)	575	375	0	0	0
Quartz #3 (grain)	0	0	0	0	0
Deposit #4 (aggregate)	575	0	0	375	0
Layer #5 (deposit)	0	0	0	0	0

Table 7
Surface relaxivity per phase, $\rho_{2,i}$ [μm/s].

Segmented phase	Void #1	Clay #2	Quartz #3	Deposit #4	Layer #5
Void #1 (macropore)	0	0	0	0	0
Clay #2 (kaolinite)	5	0	0	3	0
Quartz #3 (grain)	4.2	3	0	3	0
Deposit #4 (aggregate)	4 ~ 18	0	0	0	0
Layer #5 (deposit)	4 ~ 18	0	0	0	0

One example of inputs for sandstone rocks was reported by AlGhamdi et al. [61]. Properties, which govern NMR transverse relaxation in saturated rocks are: (1) magnetic susceptibility of solid and fluid phases; (2) proton density of each phase; (3) bulk, effective and cross-phase interface diffusion coefficients; (4) surface relaxivity values. The choice of physical properties, partially based on our measurements and partially based on literature survey, is discussed in detail below. Surface relaxivity and diffusion components are summarised in Tables 6 and 7 respectively. Volumetric magnetic susceptibility values were measured in part directly, by using magnetic susceptibility balance Sherwood MSB Auto; linear fractional additivity of susceptibility was employed to derive property of kaolinite. The resulting assignment per phase for the case of fully decane saturated rock following phase numbering convention from the section above, in units of μSI is: $\chi(\#1) = -7.6$, $\chi(\#2) = 45.0$, $\chi(\#3) = -1.7$, $\chi(\#4) = \chi(\#5) = -9.8$.

The volumetric proton density or conversely hydrogen index (HI) here is normalised to that of bulk pure water or decane for which $HI(\#1)$ is equal to 1. On the other side, the hydrogen density of quartz grains, $HI(\#3)$, is assumed to be precisely 0. Due to limited resolution micro-CT images capture kaolinite phase as a relatively uniform semi-solid/semi-void intermediately attenuated substance. Here we assume $HI(\#2) = 0.5$, which is close to published values. Recent studies agrees on kaolinite porosity values of about 42% [62], 42 ± 13.5% is given in [63]. Earlier diagenetic kaolinite porosity was reported being anywhere between 15 and 61% depending on texture, with average value of 43% [64]. However, for vermicular type sightly higher values of 45–50% are typical. The porosity of kaolinite phase is specifically important in our work since relaxation in this phase is an intended reference for aged cores where another clay-like phase of deposited asphaltenes may appear.

The input diffusion coefficient value in the kaolinite phase is an effective property, which depends on bulk diffusion coefficient, tortuosity and porosity: $D_e(\#2,2) = D_o(\#1)\phi/\tau$. The bulk diffusion coefficient of n-decane is $D_o(\#1,1) = 1250\,\mu m^2/s$ at 20 °C). Following the definition above, porosity of kaolinite is equal to $HI(\#2) = 0.5$ and tortuosity τ may be approximated by a granular pack of equal porosity ~1.6 [66]. Thus, we estimated the effective diffusion coefficient in kaolinite as $D_e(\#2,2) = 375\,\mu m^2/s$. Published data of diffusion in kaolinite [65] supports our estimate of $D_e(\#2,2)$. Effective diffusion coefficient at 23 °C estimated from their low-temperature set (10 °C) is about $365\,\mu m^2/s$, Fig. 6. Their higher temperature set obtained at 30 °C shows anomalously high diffusion of decane in kaolinite (about 5 times faster than bulk fluid) and we do not consider this result applicable to our system. We reproduce these two sets and our attempt to evaluate D_e at 23 °C. To

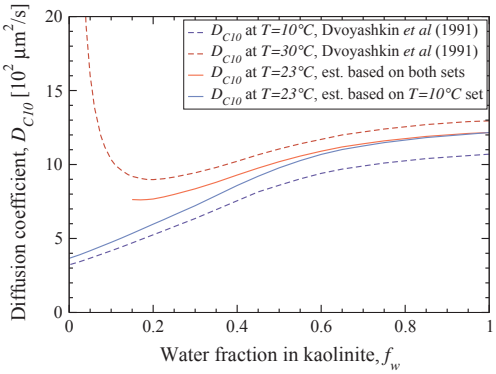

Fig. 6. Diffusion coefficient of n-decane in kaolinite at 10 °C and 30 °C [65] and the diffusion estimate at 23 °C based on their data.

conserve diffusion flux at the interface between macro-pore and kaolinite phases we use a common diffusion coefficient in both directions calculated as harmonic mean of two, $D_e(\#1,2) = D_e(\#2,1) = 575\,\mu m^2/s$. The problem of diffusion at the interface in context of simulated diffusion-dominated transport on a grid is discussed in [67,68].

Approaches to determine surface relaxivity include:

(a) matching MICP pore aperture to T_2 relaxation distributions (by various ways - optimum fit (maximising cross-correlation between throat radius and relaxation components), log-mean or mode match, etc.) [69,70];
(b) time-dependent diffusion in the limit of short diffusion time [40];
(c) matching simulated NMR relaxation response to experiment using micro-CT rock representation [71,61].

NMR relaxation and MICP distributions can be related to each other if the fast diffusion relaxation regime and negligible diffusion coupling conditions hold; and most importantly, the correspondence exists between pore-throat and pore-body sizes. For the Benththeimer sandstone these conditions hold. We employed approaches (a) and (c), which resulted in identical surface relaxivity estimates. Several values of surface relaxivity ρ_2 of a fully water saturated Bentheimer sandstone have been previously published: 7.6 μm/s [72], 9.3 μm/s [71], 9.5 μm/s [73], 9.9 μm/s [74] and a significantly higher value of 15.4 μm/s [75]. Matching of simulated and numerical T_2 responses conducted in this work resulted in a surface relaxivity of water to quartz of 9.3 μm/s. Bentheimer sandstone has another minor though relatively important phase – that is kaolinite. Reported surface relaxivity of clays is generally low, which still may enhance relaxation significantly due to their high surface-to-volume ratio. Kaolinite to water surface relaxivity values of 0.7, 1.4 and 1.8 μm/s were reported in [76–78] respectively.

A surface relaxivity of kaolinite to water of 6.0 μm/s was determined by matching numerical and experimental T_2 relaxation distributions and reported in [74]; here we use 5.0 μm/s (to decane). Relaxation within the bulk kaolinite phase is considered to be an effective property having particular relaxation rate constant, $T_2(\#2) = 25$ ms [74]. The same value is applied in the current work for the case of the kaolinite-decane system. Another bulk phase, asphaltene accumulations (see SEM depicted on Fig. 9) receives $T_2(\#2) = 40$ ms and relaxivity $\rho_2(\#4)$ equal to that of a surface layer $\rho_2(\#5)$. The actual value of surface relaxivity of asphaltene deposits is subject of this study.

5. Results

5.1. Beadpacks

Visual inspection of the beadpacks aged in crude oil shows only a slight change in beads colour (Fig. 2[g]); four synthetic oils changed

Table 8
Physical properties and relaxivity of beadpacks aged in various oils over 14 days.

Beadpack sample	Ref.1	Ref.2	OM.4	OM.3	OM.2	OM.1	OM.0	Crude
N beads, estimated [pcs]	5114	5260	5059	5135	5092	5107	5076	5006
S/V calculated [μm^{-1}][a]	0.0068	0.0070	0.0069	0.0072	0.0070	0.0070	0.0071	0.0070
S/V evaluated, $3/r$ [μm^{-1}][b]	0.0255	0.0255	0.0255	0.0255	0.0255	0.0255	0.0255	0.0255
Relaxation time, T_{2LM} [ms]	1028.9	1049.6	1023.1	1007.6	1010.4	1011.8	1026.7	1064.4
Relaxivity ρ_2 [$\mu m/s$]	3.41	3.50	3.56	3.94	3.73	3.63	4.17	2.99
ρ_2 evaluated [$\mu m/s$][c]	9.01	9.23	9.39	10.38	9.85	9.57	11.01	7.89

[a] Calculated surface-to-volume S/V values based on known weight of beads and assumed uniform shape and size.
[b] Evaluated S/V come from surface area of inscribed spheres to account for bulk and surface relaxation processes.
[c] Evaluated ρ_2 values take into account the slow diffusion relaxation regime.

beads colour to medium brown (Fig. 2[b–e]) and ageing with oil OM.0 resulted in the strongest change of colour, to dark brown (Fig. 2[f]). Relaxation time measurements were used to calculate surface relaxivity as a function of oil type used for ageing, Table 8. Oil OM.0 demonstrates the strongest increase of relaxivity of the aged beadpack – by 40%. Oils OM.2, OM.3 show the moderate relaxivity increase – by 10%, oil OM.1 – by meagre 5% and mixture with the highest fraction of asphaltenes shows the least increase of relaxivity, by 3%. Ageing in natural crude oil resulted in a decrease of relaxivity by 15%, which may be explained by the nature of deposition process likely involving wax.

5.2. Sandstone cores

Visual inspection of the cores aged in oil OM.1 (after being cleaned and dried) reveals their stronger and earlier colour change to dark brown-black comparing to cores aged with oils OM.2 and OM.3, Fig. 3. This has a certain correspondence to amount of precipitate and possibly to precipitate type (Fig. 12). Interestingly, the amount of precipitate and degree of colour change anti-correlates to the initial amount of asphaltenes in synthetic oils. To elucidate the qualitatively characteristic difference in deposition processes between three systems (Bentheimer cores aged in three synthetic oils) we use scanning electron microscopy. Images of cores were obtained using a FEI Nova NanoSEM 450 field-emission scanning electron microscope (FE-SEM) at the Mark Wainwright Analytical Centre (MWAC), UNSW. Samples were platinum coated. Fig. 8[a] shows clean quartz grain surface of a reference sample and [b–d] precipitate coverage with small to moderate accumulations of asphaltene-resin micelles (13 days of ageing in oils OM.1, OM.2 and OM.3).

Oil OM.1 creates the largest aggregates deposited on grain surfaces (10–15 μm across), oil OM.2 causes smaller and flat deposits about 5–6 μm across, and oil OM.3 creates the smallest deposits of about 2–3 μm. These aggregates are made of micelles of 200–300 nm across. Published values of micelle size vary greatly, from nano- to micron-scale. Generally, the agreed size of asphaltenes particles in very diluted toluene solution is between 5 and 25 nm [79], which creates larger flocs of 300 nm in diameter in higher heptane/toluene ratios [80] and may be well in excess of a micron [81]. Yet noteworthy, these micelles are porous. Note that the deposition layer on the quartz grain corresponding to a core aged with oil OM.3 is not continuous, but contains about circular shaped spots of exposed quartz 0.5–1 μm across, Fig. 8[d].Similarly, a core aged in oil OM.1 shows rounded gaps in a deposited layer Fig. 7[a–d]. The coverage θ_a in both cases is approximately 70%. A similar pattern of precipitate was reported in [82] and the average thickness of deposit on a glass substrate between 17 and 69 nm (as a result of 6 days of ageing at 60 °C). At certain conditions circular spots of exposed substrate formed by water micro-lenses, 0.2–1.2 μm in diameter, were formed. Despite that they used a variety of cleaning (rinsing) procedures, coverage θ_a was incomplete in all cases, varying between 10% and 70%. Asphaltene accumulation process in sandstones certainly respects pore geometry and growth starts in crevices and pore corners. Accumulations in the pore crevices are rare for the cores aged over 13 days, but occasionally of significant size, Fig. 9[a]. They become more common in cores aged over longer time, e.g. after 52 days in oil OM.3 Fig. 9[b]. Cores aged that long have many pores completely clogged with deposits. Interestingly, clogging aggregates formed by ageing in oil OM.1 show low primary porosity and appear to be made of a kind of melted spherical particles of 1.5–2.5 μm in size, Fig. 10[a]. Pore-clogging aggregates accumulated as a result of ageing in OM.2 are represented by fine particles of 300–500 nm, which exhibit a variety of pore-size scales and very high porosity, Fig. 10[b]. Pore-filling kaolinite in Bentheimer tends to adsorb a limited amount of asphaltene micelles on negatively charged hydroxylated edge surfaces, while basal surfaces remain clean.

5.3. Effect of oil composition

Among indicators commonly used to predict asphaltene deposition are asphaltene-to-resin ratio (A/R) and SARA-based CII (Colloidal Instability Index) [83]. If A/R is less than 0.35 the feed is considered to be stable. All oil mixtures used in this work have A/R close to the 0.35 threshold, Table 3. The crude oil sample has A/R of 0.23, which corresponds to a stable feed, and accordingly, demonstrates very weak deposition rate and wettability alteration capacity. Another measure of stability, CII, indicates stable oil if $CII < 0.7$, very instable if $CII > 0.9$, and values in between correspond to a moderate degree of instability. The stability of asphaltenes relates to deposition likelihood and potentially to observed change of relaxation time of saturated bead packs (Table 8) and Bentheimer cores. We observed a strong dependency of decane affinity to aged bead packs and sandstone cores on oil composition used for ageing. For the moderate length of ageing (2–3 weeks), asphaltenes of the most instable oils demonstrate highest adsorption potential (OM.0 with $CII = 1.12$ for bead packs and OM.1 with $CII = 1.03$). The effect of ageing can be evaluated using relaxivity change relative to non-aged core ($d\rho_n$ is introduced earlier above). Expectedly, the relaxivity increase is proportional to general CII – the higher CII the stronger surface relaxivity increase. Published data show that crude oil with lower asphaltene content can also have a higher tendency to precipitate comparing to asphaltene-rich oils [19]. This also applies to our results, which confirm that oils with high CII and low asphaltene content are more prone to asphaltene deposition.

5.4. Relaxation time

Experimental T_2 distributions of oils and variously aged cores are summarised in Fig. 11. Oils with a low to moderate amount of bitumen component (OM.0, OM.1 and OM.2) show similar T_2 relaxation time distributions. The T_2 distribution of oil OM.3 is shifted towards a shorter relaxation time and more similar to one of concentrated bitumen solution in toluene (oil OM.4). T_2 distributions of aged cores saturated with decane show a clear difference depending on oil used for ageing, Fig. 11[b–d].

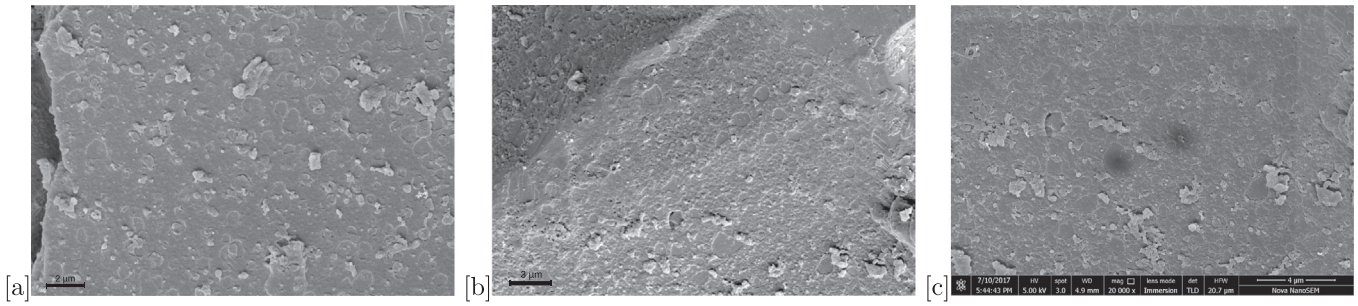

Fig. 7. [a-c] FESEM images acquired at 20,000x magnification shows partially covered surface of quartz grains of a sample aged over 13 days using oil OM.1 (coverage θ_a~70%).

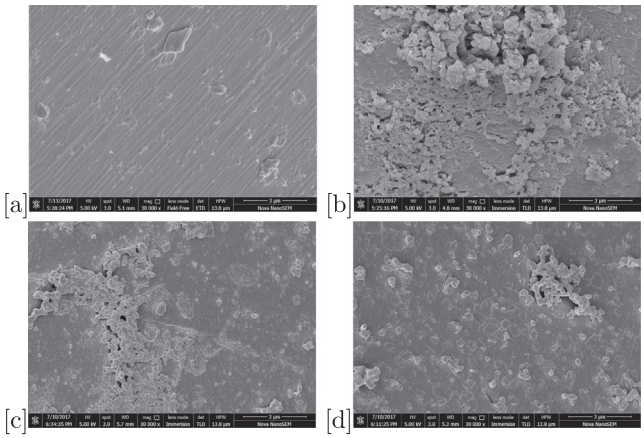

Fig. 8. FESEM images acquired at 30,000-fold magnification show [a] reference quartz grain surface; deposition and coverage of grain surface after 13 days of ageing in [b] oil OM.1, [c] oil OM.2 and [d] oil OM.3, note the exposed quartz surface.

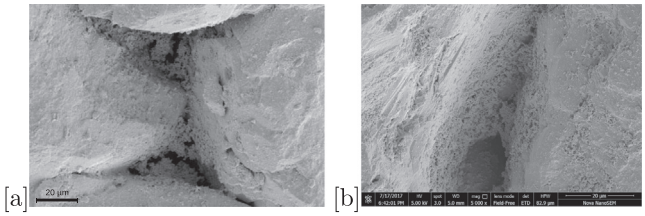

Fig. 9. FESEM images demostrating developed accumulations in pore crevices: [a] in a core aged over 13 days in oil OM.2 (such pores are rare), a segment of a 1000× magnification image; [b] in a core aged over 52 days in oil OM.3 (such pores are quite frequent), 5000x magnification.

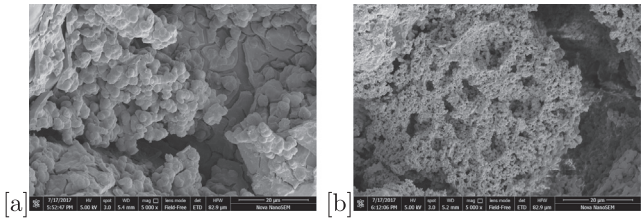

Fig. 10. FESEM images obtained at 5000× magnification show aggregates in nearly completely clogged pores after 52 days of ageing in [a] oil OM.1; [b] oil OM.2.

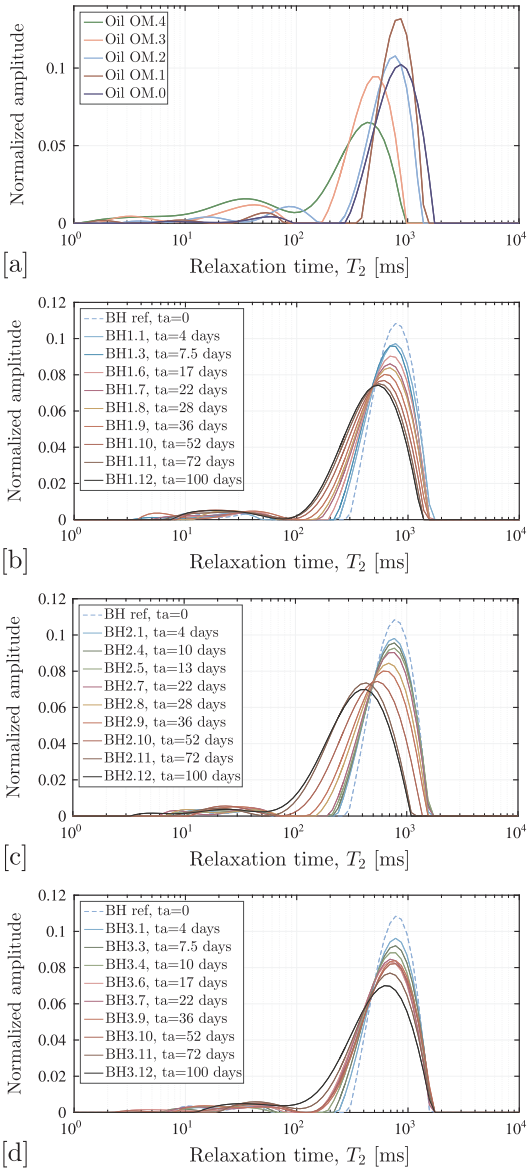

Fig. 11. T_2 distributions of [a] synthetic oils mixed with different proportions of bitumen (Tables 2–5); Bentheimer plugs aged over 0 up to 100 days in three oils: [b] oil OM.1 (BH 1.1–1.12); [c] oil OM.2 (BH 2.1–2.12); [d] oil OM.3 (BH 3.1–3.12).

T_2 distributions of cores aged in oil OM.2 shift with ageing towards short relaxation time stronger than those aged in oil OM.1, while distributions of cores aged in oil OM.3 show relatively little change until late ageing time (70 + days). The evolution and log-mean values of these T_2 distributions are shown in Fig. 12[a]. Cores aged in oil OM.3 (of a higher asphaltene content and lower *CII*) show a slower and near linear increase of relaxation over ageing time. Relaxation change of cores aged in two other oils show the existence of saturation times at about 70–80 days. These trends inversely correspond to specific adsorption of asphaltenes and pore space lost to deposition, Fig. 12[b,c].

We used relaxation data obtained with four different t_E values (100, 200, 400 and 800 μs) to estimate significance of effective internal gradients reported as normalised values (relative to non-aged) sample, Fig. 12[e], which remain nearly constant over ageing time. Thus, the

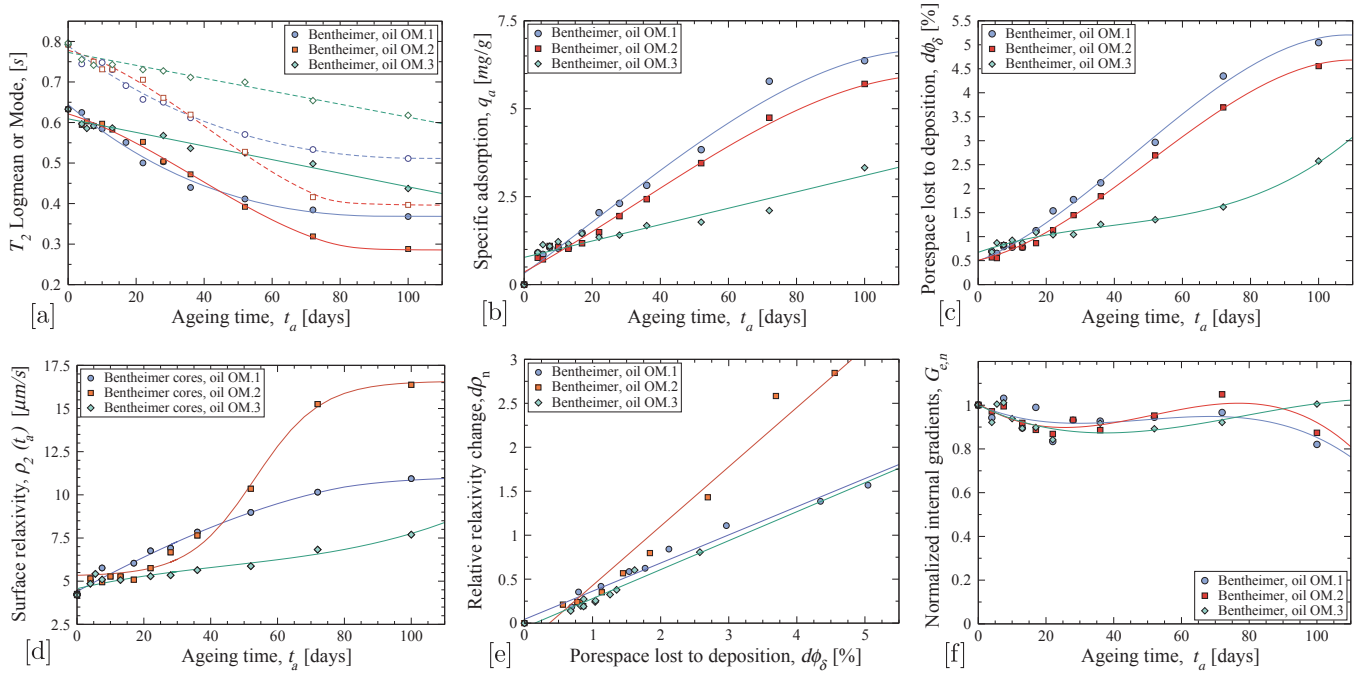

Fig. 12. [a] Log-mean (solid lines, filled symbols) and mode (dashed lines, open symbols) of T_2 relaxation time distributions measured on three sets of cores aged in oils OM.1, OM.2 and OM.3. [b] Specific adsorption of asphaltenes q_a measured from weight gain of cores over ageing time relative to initial weight of cores. [c] Pore space fraction of cores $d\phi_\delta$ lost due to deposition determined from cores weight gain relative to porosity. [d] Change of effective surface relaxivity ρ_2 over ageing time. [e] Correlation of $d\phi_\delta$ to relative relaxivity change, $d\rho_n(t_a)$. [f] Evolution of (normalised) effective internal gradients over ageing time calculated from T_2 distributions acquired with t_E = 100 and 800 μs (before ageing $G_{e,n}$ = 1).

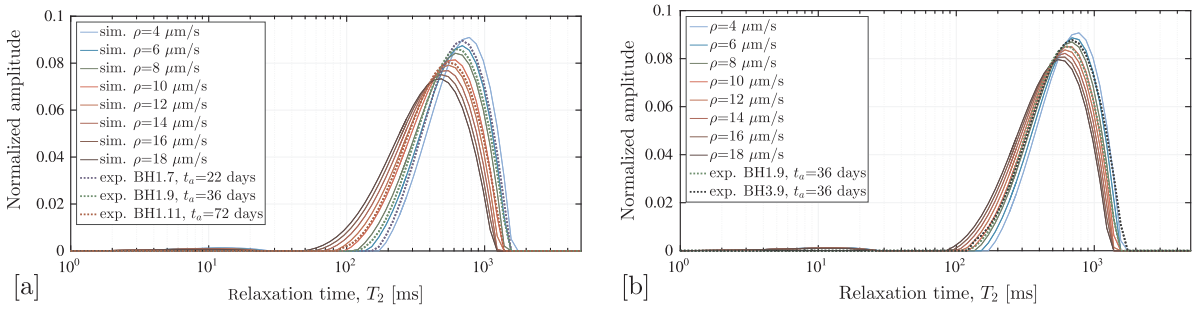

Fig. 13. Simulated T_2 distributions of 100% decane saturated Bentheimer for two deposition scenarios: [a] uniform surface coverage (constant relaxivity is changed from 4 to 18 μm/s); [b] 50% surface coverage. Several experimental T_2 distributions are shown for comparison.

change in relaxation time distributions is attributed primarily to change of surface relaxivity and pore space morphology.

Note, that the surface relaxivity evolution over aging time per individual oil is very different to related adsorption rates: the higher specific asphaltene adsorption from oil OM.1 corresponds to a nearly linear and moderate increase of surface relaxivity with a late-time saturation region - a Γ-shaped Type I adsorption process. On the other hand, OM.2 responsible for lower rate of asphaltene deposition, leads to a different type relaxivity dynamics – *S*-shaped Type II/IV curve with three distinctive elements: the slow relaxivity growth up to 40 days of ageing, fast relaxivity growth (40–80 days) and saturation region with slowing down rate after 80 days.

For 72 days of ageing time the surface relaxivity of cores aged in low asphaltene oil OM.1 increases by 2.4-fold (from 4.2 to 10.2 μm/s), ageing in medium asphaltene oil OM.2 increased relaxivity by a factor 3.6 (to 15.3 μm/s) and ageing in high asphaltene oil OM.3 increased relaxivity by a factor 1.6 (to 6.8 μm/s). Relaxivity and asphaltene adsorption rates correlate near linearly, Fig. 12[e] with identical slope for systems with oils OM.1 and OM.3 and two stronger relaxivity increase for the similar amount of adsorbed asphaltenes for the system aged in oil OM.2. The enhanced decline of relaxation rate interpreted as increase of effective surface relaxivity may be caused by clogging and diffusional coupling of the clay-like regions to remaining open pore space. T_2 relaxation exchange technique suits well for quantitative characterisation of diffusional magnetisation exchange. The coverage θ_a can be evaluated using simulated relaxation experiments by comparing experimental T_2 distribution with the set of simulated responses, which mimic uniform Fig. 13[a] or partial coverage and relaxivity [b]. For the samples aged with oil OM.1 over 22, 36 and 72 days a match is obtained with the following relaxivity values (experiment vs simulation), μm/s: BH1.7: 6.8 vs 5.5; BH1.9: 7.8 vs 7.0; BH1.11: 10.2 vs 11.0; non-aged core: 4.2 vs 4.2. Assuming additivity of fractional relaxation responses for non-altered and altered surfaces, the coverage of BH1.7 is ~35%; BH1.9: ~60%; BH1.11: ~100%. It can be tested against simulations performed with 50% of solid surface altered with different relaxivities. For the core BH1.9 simulation and experiment would match if 50% of solid surface accept a relaxivity of 10.5 μm/s. One can see that the experimental distribution overlaps with the simulated curve corresponding to ρ_2 = 10 μm/s, Fig. 13[b].

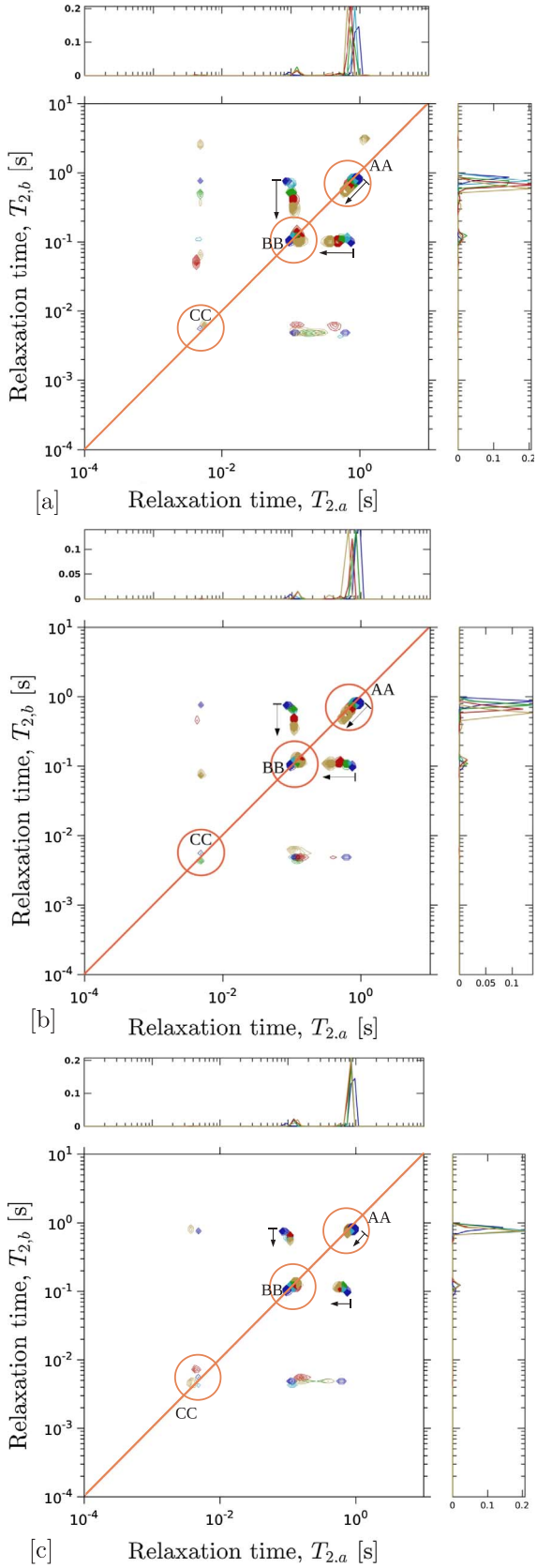

Fig. 14. Composite T_2-store-T_2 maps combining five responses of 100% decane saturated Bentheimer plugs: reference, not aged (dark blue), aged over 4 days (light blue), aged over 22 days (green), aged over 36 days (red), aged over 52 days (pale yellow) with oils [a] OM.1; [b] OM.2; [c] OM.3.

5.5. Relaxation exchange

Fig. 14[a–c] shows composite T_2-store-T_2 maps containing five overlapped maps each, where colours correspond to a reference core and four aged cores (4, 22, 36, 52 days). Similar to T_2 relaxation, the REXSY experiment detects the shift of the main relaxation peak 'AA' towards shorter relaxation time, which here is directly attributed to surface relaxivity change, while the magnetisation exchange component of a signal appears as off-diagonal cross-peaks ('AB, BA'; 'AC','CA'; 'BC','CB').

The part of a total amplitude of a REXSY signal other than main peak 'AA' and half amplitude of 'AB'/'BA' peaks can be related to magnetisation originating from micro-porosity and diffusional leak into macro-porous regions. Relating this fractional signal measured on aged core to non-aged reference one, we can calculate increase of would be microporosity (of asphaltene aggregates), following Eq. (1). Since the total amount of adsorbed asphaltene is known, we now have information about the amount of asphaltene deposited in a layer V_{layer} and as aggregates V_{agg}. Assuming covering layer of a uniform thickness this also provides adjusted layer thickness, $\delta_{a,layer}$.

Using XRD/XRF data and micro-CT image analysis we derived the following major phases of Bentheimer (in vol.% of total bulk rock volume): quartz and K/Na-feldspar together – 74.76% (including 2.5% of feldspar); kaolinite – 1.64% (solid) and 1.09% (void); macro-pores 22.51%. Estimated porosity of kaolinite phase using approach based on fractional REXSY signal of saturated reference sample is about 40%, which is slightly lower than the default value used in simulation. The underlying assumption is that feldspar grains and quartz grain contacts have no contribution to observed signal, which we interpreting as micro-porosity. The amount of asphaltenes deposited in the form of aggregates over ageing time closely follows the evolution pattern of fractional REXSY signal depicted in Fig. 15[a] where porosity of aggregates ϕ_{asph} is assumed to be constant. We have an excess of unknowns and the precise ϕ_{asph} value can be determined by involving simulated relaxation experiment or other source. It can be well constrained by the simple condition: $V_{agg} \leqslant V_{a,total}$, i.e. the solid fraction of asphaltenes in the form of aggregates cannot exceed the total amount of adsorbed asphaltenes. This provides an estimate of ϕ_{asph} ~0.85. These aggregates indeed are very porous, see FESEM Fig. 8[b], Fig. 10[b].

The evolution of a solid asphaltene fraction coating grains presented as a fraction of core bulk volume is shown in Fig. 15[c]. The corresponding thickness of uniform layer is shown in Fig. 15[d]. The underlying assumption is that the kaolinite pore-space is not plugged with asphaltenes and the thin asphaltene nano-scale layer has no detectable NMR intensity. Note, that the adsorbed layer from oil OM.3 is the thinnest and remains constant ~70 nm over the most part of ageing time, 15–65 days.

Lastly, the curves in Fig. 12 and Fig. 15 are given to guide the eye While a substantial effort has been applied to obtain a good quality fit with minimum residual sums, it is important to state that a physical meaning of these functions (typically power-law or high degree polynomials) is not expected. Here we consider that the qualitative comparison of trend shapes is fully sufficient.

6. Discussion

Measured adsorption and surface relaxivity change over ageing time in saturated sandstone shows that the process is specific to the chemical composition of ageing oil. In particular, oil with the highest asphaltene content (OM.3) demonstrates the lowest asphaltene adsorption capacity, while oil OM.1, which is different from the former only in a factor 2.5 lower asphaltene fraction, shows much higher adsorption rate. While this result might sound counter-intuitive, it is exactly in line with reported field observations - asphaltene precipitation problems are typical in reservoirs containing light to medium oils with low asphaltene content and heavy crudes that contain a larger amount of asphaltene

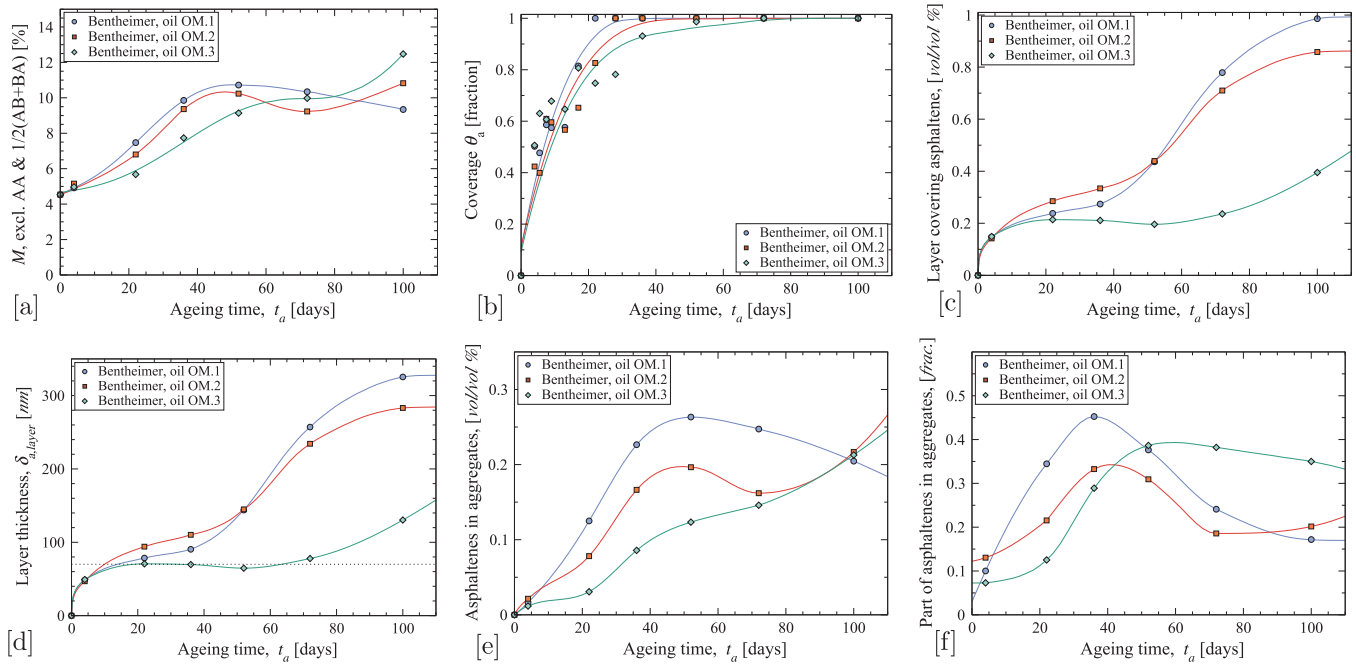

Fig. 15. [a] Evolution of AA peak and half of AB + BA peaks of T_2-T_2 maps during ageing time; [b] coverage θ_a calculated in assumption of a uniform nano-layer using surface area calculated from micro-CT image and relaxation data from CPMG experiment; [c] part of total adsorbed asphaltenes in a form of covering layer calculated from T_2-T_2 and presented as percentage of a sample volume (also 1 vol/vol.% corresponding to a 330 nm thick uniform layer); [d] same as [c], but data presented as equivalent uniform layer thickness, $\delta_{a,layer}$; [e] Part of adsorbed asphaltene in a form of aggregates, in percentage of sample volume; [f] Asphaltene in aggregates (same data as [e]) expressed as a fraction of total deposited volume.

have very few asphaltene precipitation problems, [84,85]. Interestingly, the high rate of asphaltene adsorption in Bentheimer aged in low asphaltene oil OM.1 does not correspond to a similar surface relaxivity increase. Indeed, surface relaxivity calculated as an effective property includes a contribution from micro- and nano-porous clay-like asphaltene-resin aggregates and diffusional magnetisation exchange with macro-porosity. Over ageing time and rinsing step the two adsorption processes occur in parallel: coverage of the grain surfaces and pore clogging. Exposure of sandstone to synthetic oil changes wettability to mixed-wet state very quickly. A water imbibition test of a reference core resulted in displacement of 36% of decane initially fully saturating core (in line with published value of 44% [86]). Four days of ageing and subsequent ageing steps resulted in about 1% of oil displacement, which indicates at least mixed-wet conditions. Selection of oil chemistry and ageing conditions (time and temperature) creating a thin uniform grain coverage without clogging and minimum aggregates would improve the quality of core ageing step. Deficiencies of T_2 relaxation data in characterisation of clogging and diffusional coupling can be overcome using T_2 relaxation exchange technique.

7. Conclusion

The proposed approach – a set of NMR relaxation and relaxation-exchange experiments combined with simulated relaxation responses enables to identify evolution of asphaltene deposition over ageing time. We demonstrated that low-field NMR time-series relaxation techniques are applicable to monitor asphaltene adsorption and rock wettability state by detecting surface relaxivity change. The relaxation exchange technique provides additional quantitative information about volumetric fraction of micro- and macro-porosity by explicitly separating diffusionally coupled magnetisation components. Being calibrated to a known micro-porous environment (kaolinite), it provides estimates of asphaltene solid fractions adsorbed in a covering layer and deposited as aggregates and elements of pore space morphology change: coverage, layer thickness, porosity of aggregates and fraction of clogged pore space. The rate of these two adsorption processes strongly depends on chemical composition of ageing oils. The nature of adsorption processes can be characterised using type-curves (isotherms). The chemical composition of bitumen-based synthetic oils has similar effect on deposition likelihood as field examples reported in literature – oils with high asphaltene content are less prone to deposition. Synthetic oils offer an extra means of control (in addition to temperature, time, etc.) on degree and pattern of wettability alteration by adjusting chemical composition. This allows a more thorough design of wettability reversal steps in laboratory core analysis.

Understanding the dynamics of wettability alteration enhances our ability to reproduce reservoir conditions before performing core flooding tests and aids to ensure representativeness of laboratory data. It also provides a pathway for the solution of a forward pore-scale wettability problem of unknown spatial distribution and magnitude of surface relaxivity by simulated NMR relaxation experiment. The current study has been performed on well defined samples of simple morphology and mineralogy. In future work we consider to extend the approach to sandstones with diverse clay types and complex morphology, as well as to carbonates.

Acknowledgements

The authors acknowledge the Australian Research Council and the member companies of the ANU/UNSW Digital Core Consortium for their support. CHA thanks the Australian Research Council for a Future Fellowship (FT120100216). This research was undertaken with the assistance of resources and services from the National Computational Infrastructure (NCI), which is supported by the Australian Government. Authors wish to thank Dr. Yin Yao from MWAC UNSW for assisting with FESEM.

References

[1] Speight JG. The application of spectroscopic techniques to the structural analysis of coal and petroleum. Appl. Spectrosc. Rev. 1971;5(1):211–63.
[2] Mullins OC. The modified Yen model. Energy Fuels 2010;24:2179–207.
[3] Amott E. Observations relating to the wettability of porous rock. Trans AIME 1959;216:156–62.
[4] Ma S, Zhang X, Morrow NR, Zhou X. Generalization of wettability from spontaneous

imbibition measurements. J Can Petrol Technol 1999;38(13):1–8.
[5] Bassioni G, Taqvi ST. Wettability studies using zeta potential measurements. J Chem 2015. pages 743179:1–6.
[6] Wang Y, Ma L, Bai B, Jiang G, Jin J, Wang Z. Wettability alteration of sandstone by chemical treatments. J Chem 2013;845031:1–8.
[7] Kim ST, Boudh-Hir M-E, Monsoori GA. The role of asphaltene in wettability reversal. In: Proc. SPE Ann. Tech. Conf. & Exhib., pages 799–809, New Orleans, USA, September 23–26; 1990. SPE 87009.
[8] Graue A, Aspenes E, Bogn T, Moe RW, Ramsdal J. Alteration of wettability and wettability heterogeneity. J Petr Sc Eng 2002;33:3–17.
[9] Fleury M, Deflandre F. Quantitative evaluation of porous media wettability using NMR relaxometry. Magn Reson Imag 2003;21(3–4):385–7.
[10] Looyestijn W, Hofman J. Wettability-index determination by nuclear magnetic resonance. SPE Res Eval Eng 2006;9(2):146–53.
[11] Chen J, Hirasaki GJ, Flaum M. Effect of OBM on wettability and NMR responses. J Petr Sci Eng 2006;52:161–71.
[12] Johannesen E, Howard J, Graue A. Evaluation of wettabilty distributions in experimentally aged core. In: 22nd Int. Symp. Soc. Core Analysts, pages 1–12, Abu Dhabi, UAE; October 2008. SCA2008-17.
[13] Al-Mahrooqi SH, Grattoni CA, Muggeridge AH, Jing XD. Pore-scale modelling of NMR relaxation for the characterization of wettability. J Petr Sci Eng 2006;52:172–86.
[14] Blunt MJ. Pore level modelling of effects of wettability. Soc Pet Eng J 1997;2:449–510.
[15] Arns CH, Sheppard AP, Saadatfar M, Knackstedt MA. Prediction of permeability from NMR response: surface relaxivity heterogeneity. In: 47th Ann. Logg. Symp. pages 1–13, Veracruz, Mexico, June 2006. Soc. of Petrophys. & Well Log Analyst.
[16] Ryu S. Effect of inhomogeneous surface relaxivity, pore geometry and internal field gradient on NMR logging: Exact and perturbative theories and numerical investigations. In: 50th Ann. Logg. Symp. pages 1–16, The Woodlands, Texas, June 21–24 2009. Soc. Petrophys. & Well Log Analyst.
[17] Keating K, Knight R. The effect of spatial variation in surface relaxivity on nuclear magnetic resonance relaxation rates. Geophysics 2012;77(5):E365–77.
[18] Yan J, Plancher H, Morrow NR. Wettability changes induced by adsorption of asphaltenes. SPE Prod Facil 1997;12(4):259–66.
[19] Minssieux L, Nabzar L, Chauveteau G, Longeron D, Bensalem R. Permeability damage due to asphaltene deposition: experimental and modeling aspects. Rev IFP 1998;53(3):313–27.
[20] Sing KSW, Everett DH, Haul RAW, Moscou L, Pierotti RA, Rouquérol J, Siemieniewska T. Reporting physisorption data for gas/solid systems with special reference to the determination of surface area and porosity. Pure Appl Chem 1985;57(4):603–19.
[21] Fowler RH, Guggenheim EA. Statistical thermodynamics. New York, USA: Cambridge University Press; 1949.
[22] Hoepfner MP, Limsakoune V, Chuenmeechao V, Maqbool T, Fogler HS. A fundamental study of asphaltene deposition. Energy Fuels 2013;27:725–35.
[23] Wang J, Buckley JS, Creek JL. Asphaltene deposition on metallic surfaces. J Dispers Sci Technol 2004;25(3):287–98.
[24] Zanganeh P, Ayatollahi S, Alamdari A, Zolghadr A, Dashti H, Kord S. Asphaltene deposition during CO_2 injection and pressure depletion: a visual study. Energy Fuels 2012;26:1412–9.
[25] Zhuang Y, Goharzadeh A, Lin YJ, Yap YF, Chai JC, Mathew N, et al. Three dimensional measurements of asphaltene deposition in a transparent micro-channel. J Petr Sci Eng 2016;145:77–82.
[26] Zhao Y, Wand T, Song Y, Liu Y, Dong B, Zhu N. Visualization of asphaltene deposition effects on porosity and permeability during CO_2 flooding in porous media. J Visualization 2016;19(4):603–14.
[27] Kumar M, Fogden A. Patterned wettability of oil and water in porous media. Langmuir 2010;26(6):4036–46.
[28] Treiber LE, Archer DL, Owens WW. A laboratory evaluation of wettability of fifty oil-producing reservoirs. Soc Pet Eng J 1972;12(6):531–40.
[29] Dashti H, Zanganeh P, Ayatollahi S. The comparison between heavy and light oil asphaltene deposition during pressure depletion and CO_2 injection at reservoir condition, a visual laboratory study. In: 41st Chemeca Conf., Brisbane, Australia, September 2013. IEA.
[30] Farooq U, Tweheyo MT, Sjöblom J, Ye G. Surface characterization of model, outcrop, and reservoir samples in low salinity aqueous solutions. J Disp Sci Tech 2011;32:519–31.
[31] Halisch M, Vogt E, Müller C, Cano-Odena A, Pattyn D, Hellebaut P, van der Kamp K. Capillary flow porometry – assessment of an alternative method for the determination of flow relevant parameters of porous rocks. In: 27th Int. Symp. Soc. Core Analysts, pages 1–12, Napa Valley, CA, USA, September 2013. SCA2013-007.
[32] Bazaikin Y, Gurevich B, Iglauer S, Khachkova T, Kolyukhin D, Lebedev M, Lisitsa V, Reshetova G. Effect of CT image size and resolution on the accuracy of rock property estimates. J. Geophys. Res.: Solid Earth 2017;122(5):3635–47.
[33] Hürlimann Martin D. Effective gradients in porous media due to susceptibility differences. J Magn Res 1998;131:232–40.
[34] Shikhov I, Arns CH. Evaluation of capillary pressure methods via digital rock simulations. Transp Porous Media 2015;107(2):623–40.
[35] Siena M, Guadagnimi A, Riva M, Bijeljic B, Pereira Nunes JP, Blunt MJ. Statistical scaling of pore-scale Lagrangian velocities in natural porous media. Phys Rev E 2014;90(023013):1–8.
[36] Shikhov I, d'Eurydice MN, Arns J-Y, Arns CH. An experimental and numerical study of relative permeability estimates using spatially resolved T_1-z NMR. Transp Por Med 2017;118(2):225–50.
[37] Brownstein KR, Tarr CE. Importance of classical diffusion in NMR studies of water in biological cells. Phys Rev A 1979;19:2446–53.
[38] Kleinberg RL, Horsfield MA. Transverse relaxation processes in porous sedimentary rock. J Magn Res 1990;88:9–19.
[39] Lonnes S, Guzman-Garcia A, Holland R. NMR petrophysical predictions on cores. In The 44th Ann. Logg. Symp., Galveston, USA, June 2003. Soc. of Petrophys. & Well Log Analysts.
[40] Slijkerman WFJ, Hofman JP. Determination of surface relaxivity from NMR diffusion measurements. Magn Reson Imaging 1998;16(5/6):541–4.
[41] Shikhov I, Arns CH. Temperature-dependent oxygen effect on NMR $D-T_2$ relaxation-diffusion correlation of n-alkanes. Appl Magn Reson 2016;47(12):1391–408.
[42] Singer PM, Asthagiri D, Chapman WG, Hirasaki GJ. Molecular dynamics simulations of NMR relaxation and diffusion of bulk hydrocarbons and water. J Magn Res 2017;277(15–24).
[43] Carr HY, Purcell EM. Effects of diffusion on free precession in nuclear magnetic resonance problems. Phys Rev 1954;94:630–8.
[44] Meiboom S, Gill D. Modified spin-echo method for measuring nuclear relaxation times. Rev Sci Instrum 1958;29:688–91.
[45] Lawson CL, Hansen RJ. Solving least squares problems. New-Jersey: Prentice-Hall; 1974.
[46] Hansen PC. Numerical tools for analysis and solution of Fredholm integral equations of the first kind. Inverse Prob 1992;8(6):849–72.
[47] Stejskal EO, Schaefer J. Data routing in quadrature FT NMR. J Magn Res 1974;13(2):249–51.
[48] Lee J-H, Labadie C, Springer Jr. CS, Harbison GS. Two-dimensional inverse Laplace transform NMR: altered relaxation times allow detection of exchange correlation. J Am Ceram Soc 1993;115:7761–4.
[49] McDonald PJ, Korb J-P, Mitchell J, Monteilhet L. Surface relaxation and chemical exchange in hydrating cement pastes: a two-dimensional NMR relaxation study. Phys Rev E 2005;72(011409):1–9.
[50] Washburn KE, Callaghan PT. Tracking pore to pore exchange using relaxation exchange spectroscopy. Phys Rev Lett 2006;97(175502):1–4.
[51] Venkataramanan L, Song Y-Q, Hürliman MD. Solving Fredholm integrals of the first kind with tensor product structure in 2 and 2.5 dimensions. IEEE Trans.on. Signal Process 2002;50(5):1017–26.
[52] Valori A, McDonald PJ, Scrivener KL. The morhology of C-S-H: lessons from ^{1}H nuclear magnetic resonance relaxometry. Cem Concr Res 2013;49:65–81.
[53] Mitchell J, Griffith JD, Collins JHP, Sederman AJ, Gladden LF, Johns ML. Validation of NMR relaxation exchange time measurements in porous media. J Chem Phys 2007;127(234701):1–9.
[54] Codd SL, Manz B, Seymour JD, Callaghan PT. NMR relaxation measurements of biofouling in model and geological porous media. Org Geochem 2011;42:965–71.
[55] Fleury M, Soualem J. Quantitative analysis of diffusional pore coupling from T_2-store-T_2 NMR experiments. J Coll Interf Sci 2009;336:250–9.
[56] Song R, Song Y-Q, Vembusubramanian M, Paulsen JL. The robust identification of exchange from T_2-T_2 time-domain features, verse relaxation exchange. J Magn Reson 2016;265:164–71.
[57] Song Y-Q, Zelinski L, Ryu S. Two-dimensional NMR od diffusion systems. Phys Rev Lett 2008;100(248002):1–4.
[58] Arns CH, Sheppard AP, Sok RM, Knackstedt MA. NMR petrophysical predictions on digitized core images. Petrophysics 2007;48(3):202–21.
[59] Arns CH, AlGhamdi T, Arns J-Y. Numerical analysis of NMR relaxation-diffusion responses of sedimentary rock. New J Phys 2011;13. 015004:1–17.
[60] Arns CH, Knackstedt MA, Martys N. Cross-property correlations and permeability estimation in sandstone. Phys Rev E 2005;72(046304):1–12.
[61] AlGhamdi TM, Arns CH, Eyvazzadeh RY. Correlations between NMR-relaxation response and relative permeability from tomographic reservoir-rock images. SPE Res Eval Eng 2013;16(4):369–77.
[62] Wilson MJ, Wilson L, Patey I. The influence of individual clay minerals on formation damage of reservoir sandstones: a critical review with some new insights. Clay Miner 2014;49:147–64.
[63] Sardini P, El Albani A, Pret D, Gaboreau MSiitari-KauppiS, Beaufort D. Mapping and quantifying the clay aggregate microporosity in medium- to coarse-grained sandstones using the ^{14}C-PMMA method. J Sedim Res 2009;79:584–92.
[64] Hurst A, Nadeau PH. Clay microporosity in reservoir sandstone: an application of quantitative electron microscopy in petrophysical evaluation. AAPG Bull 1995;79(4):563–73.
[65] Dvoyashkin NK, Skirda VD, Maklakov AI, Belousova MV, Valiullin RR. Peculiarities of self-diffusion of alkane molecules in kaolinite. Appl Magn Reson 1991;2(1):83–91.
[66] Dias R, Teixeira J, Mota M, Yelshin A. Tortuosity variation in a low density binary particulate bed. Sep Purif Technol 2006;51:180–4.
[67] Patankar SV. Numerical heat transfer and fluid flow. Washington D.C.: Hemisphere; 1980.
[68] Chang KC, Payne UJ. Numerical treatment of diffusion coefficients at interfaces. Numer Heat Transf A 1992;21(3):363–76.
[69] Kenyon WE, Howard JJ, Sezginer A, Straley C, Matteson A. Pore-size distribution and NMR in microporous cherty sandstones. In 30th Ann. Logg. Symp. pages 1–24, Denver, CO, USA; June 11–14 1989.
[70] Marschall D, Gardner JS, Mardon D, Coates GR. Method for correlating NMR relaxometry and mercury injection data. Number SCA1995-11 in The 9th Int. Symp.of Soc.of Core Analysts, pages 1–12, San-Francisco; September 12–14 1995.
[71] Talabi O, Alsayari S, Fern M, Riskedal H, Graue A, Blunt MJ. Pore-scale simulation of NMR response in carbonates. In The 22nd Int. Symp.of the Soc.of Core Analysts, pages 1–12, Abu Dhabi, UAE, Oct. 29-Nov.02 2008. SCA2008-30.
[72] Souza A, Carneiro G, Boyd A, Hürlimann M, Trevizan W, Coutinho B et al. Improving lab NMR petrophysical estimations by incorporating the surface

relaxivity parameter. In: 31st Int. Symp. Soc. Core Analysts, pages 1–6, Snowmass, CO, USA, August 2016. SCA2016-047.
[73] Washburn KE, Sandor M, Cheng Y. Evaluation of sandstone surface relaxivity using laser-induced breakdown spectroscopy. J Magn Reson 2017;275:80–9.
[74] Shikhov I. Integration of micro-CT and NMR-based techniques for reservoir rock characterization. Sydney, Australia: University of New South Wales; 2015. [Ph.D. thesis].
[75] Zhang Q, Lo S-W, Huang CC, Hirasaki GJ, Kobayashi R, House WV. Some exceptions to default NMR rock and fluid properties. In 39th SPWLA Ann. Logg. Symp. pages 1–14, Keystone, CO, USA; 1998.
[76] Prammer MG, Drack ED, Bouton JC, Gardner JS. Measurements of clay-bound water and total porosity by magnetic resonance logging. Log Analyst 1996;37(6):61–9.
[77] Anand V, Hirasaki GJ, Fleury M. NMR diffusional coupling: Effects of temperature and clay distribution. In: 20th Int. Symp. Soc. Core Analysts, pages 1–13, Trondheim, Norway, 12–17 September 2006. SCA2006-013.
[78] Matteson A, Tomanic JP, Herron MM, Allen DF, Kenyon WE. NMR relaxation of clay-brine mixtures. SPE Rer Eval Facil 2000;3(5):408–13.
[79] Mansur CRE, de Melo AR, Lucas EF. Determination of asphaltene particle size: influence of flocculant, additive, and temperature. Energy Fuels 2012;26:4988–94.
[80] Peréz-Hernández R, Mendoza-Anaya D, Mondragón-Galicia G, Espinosa ME, Rodríguez-Lugo V, Lozada M, Arenas-Alotorre J. Microstructural study of asphaltene precipitated with methylene chloride and n-hexane. Fuel 2003;82:977–82.
[81] Hosseini A, Zare E, Ayatollahi S, Vargas FM, Chapman WG, Kostarelos K, Taghikhani V. Electrokinetic behavior of asphaltene particles. Fuel 2016;178:234–42.
[82] Lebedeva EV, Fogden A. Nano-scale structure of crude oil deposits on water-wet substrates: dependence on aqueous phase and organic solvents. Coll Surf A: Physiochem Eng Asp 2011;380:280–91.
[83] Por N. Stability Properties of Petroleum Products. Israel Institute of Petroleum and Energy. Tel Aviv; 1992.
[84] Leontaritis K, Ali Mansoori G. Asphaltene deposition: a survey of field experiences and research approaches. J Petr Sci Eng 1988;1:229–39.
[85] de Boer RB, Leerlooyer K, Eigner MRP, van Bergen ARD. Screening of crude oils for asphalt precipitation: theory, practice, and the selection of inhibitors. SPE Prod Facil 1995;10(1):55–61.
[86] Karimaie H, Torster O, Esfahani MR. Oil recovery by water imbibition in Asmary fractured rock. In 19th Int. Symp. Soc. Core Analysts, pages 1–13, Toronto, Canada, August 2005. SCA2005-47.